Emergent Quantum Phenomena of a Noncentrosymmetric Charge Density Wave in 1*T*-Transition Metal Dichalcogenides

Cheong-Eung Ahn,[1,2,*] Kyung-Hwan Jin,[4,2,*] Young-Jae Choi,[2,3] Jae Whan Park,[2] Han Woong Yeom,[1,2] Ara Go,[5,†] Yong Baek Kim,[6,‡] and Gil Young Cho[1,2,7,§]

[1]*Department of Physics, Pohang University of Science and Technology, Pohang, 37673, Republic of Korea*
[2]*Center for Artificial Low Dimensional Electronic Systems, Institute for Basic Science, Pohang 37673, Korea*
[3]*The Anthony J Leggett Institute for Condensed Matter Theory, Department of Physics, University of Illinois at Urbana-Champaign, Urbana, Illinois 61801, USA*
[4]*Department of Physics and Research Institute of Physics and Chemistry, Jeonbuk National University, Jeonju, 54896, Republic of Korea*
[5]*Department of Physics, Chonnam National University, Gwangju 61186, Korea*
[6]*Department of Physics, University of Toronto, Toronto, Ontario M5S 1A7, Canada*
[7]*Asia-Pacific Center for Theoretical Physics, Pohang, Gyeongbuk, 37673, Korea*

(Received 15 November 2023; revised 21 March 2024; accepted 1 May 2024; published 28 May 2024)

1*T*-transition metal dichalcogenides (TMDs) have been an exciting platform for exploring the intertwinement of charge density waves and strong correlation phenomena. While the David star structure has been conventionally considered as the underlying charge order in the literature, recent scanning tunneling probe experiments on several monolayer 1*T*-TMD materials have motivated a new, alternative structure, namely, the anion-centered David star structure. In this Letter, we show that this novel anion-centered David star structure manifestly breaks inversion symmetry, resulting in flat bands with pronounced Rashba spin-orbit couplings. These distinctive features unlock novel possibilities and functionalities for 1*T*-TMDs, including the giant spin Hall effect, the emergence of Chern bands, and spin liquid that spontaneously breaks crystalline rotational symmetry. Our findings establish promising avenues for exploring emerging quantum phenomena of monolayer 1*T*-TMDs with this novel noncentrosymmetric structure.

DOI: 10.1103/PhysRevLett.132.226401

1*T*-transition metal dichalcogenides (TMDs) have exhibited a surprisingly diverse set of emergent quantum phenomena, including ultrafast manipulations of electronic states [1,2], superconductivity [3–7], Mott insulators [8–14], topological insulators [6,15,16], and spin liquids [17–21]. At the heart of all these remarkable phenomena, forming a very particular charge density wave (CDW), known as the David star (DS), is crucial, as it serves as the origin of strong electronic correlation and geometric frustration in these materials [8–12,22–25]. Indeed, several recent experiments on samples with the DS CDW have shown the opening of Mott gap and potential spin liquid behaviors [19–21,26]. These findings highlight the importance of the underlying charge order in understanding their strong correlation physics.

Scanning tunneling microscopes (STM) can probe the detailed structures of the monolayer TMD materials. In the DS CDW [Fig. 1(a)], three bright protrusions around the DS center in the top chalcogenide layer are characteristically observed [10,12], consistent with our density functional theory (DFT) simulations (see Fig. S1 [27]). However, several monolayer samples showed markedly different patterns in recent STM studies [41–43]. These experimental observations suggest the emergence of a new, alternative CDW pattern in monolayer 1*T*-TMD materials. In many CDW materials, it is well established that two or more CDW patterns can closely compete and even appear simultaneously [44–47]. Monolayer 1*T*-TMD may be no exception to this. Our recent work puts forth an alternative CDW structure for monolayer 1*T*-TMD [48], namely, the anion-centered David star (ACDS) [Fig. 1(b)], whose simulated STM images closely align with the previous experimental data (see Fig. S1 [27]).

Building upon this recent progress, here we investigate the electronic states and symmetry of the ACDS structure for a few representative materials, namely, $TaSe_2$, TaS_2, $NbSe_2$, and NbS_2. In this pursuit, we show that the ACDS structure breaks the inversion symmetry, leading to flat bands with pronounced spin-orbit couplings (SOCs). This distinctive electronic state serves as the foundation for a myriad of emerging quantum phenomena, including giant spin Hall conductivity (SHC), interaction-enabled Chern bands, and strain-engineered spin liquids with spontaneously broken crystalline rotational symmetry. Our investigation provides valuable insights into this novel noncentrosymmetric structure in monolayer 1*T*-TMD materials.

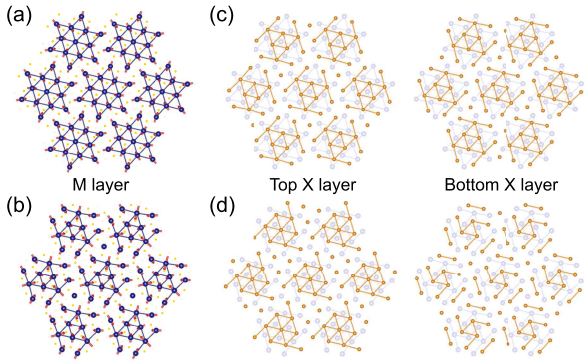

FIG. 1. ACDS vs DS structures. (a) and (b) represent the bonding networks of M atoms in the CDW states. Here, (a) is for the DS, and (b) is for the ACDS. The blue circles represent the M atoms. The arrows indicate the atomic displacement under the formation of the corresponding CDW patterns. Similarly, (c) and (d) represent the bonding networks of the top X layer (left) and the bottom X layer (right). Here, (c) is for the DS and (d) for the ACDS, respectively. The ACDS structure has distinct bonding networks of X atoms between the top and bottom X layers, leading to the broken inversion symmetry.

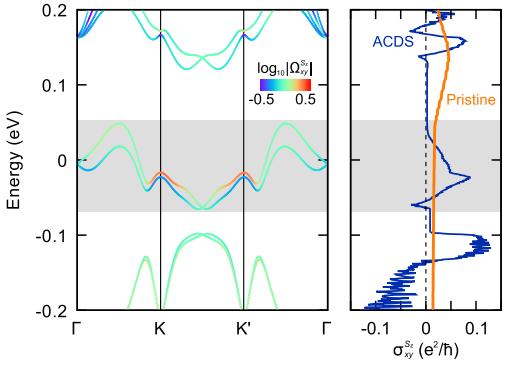

FIG. 2. SHC of ACDS 1T-TaS_2. We present the band structure and SHC of the ACDS structure in energy. In the band structure, the color scheme represents the strength of the spin Hall Berry curvature $\Omega_{xy}^{S_z}$ [27]. The shaded area represents the energy window which is attributed to the flat bands.

Structure.—The conventional DS structure naturally arises when the transition metal atoms contract toward the cation (Nb or Ta) reference atoms [Fig. 1(a)]. However, the ACDS structure arises from the contraction toward an anion (S or Se) atom instead of cation atoms [Fig. 1(b)]. Similar to the DS structure, the ACDS structure's unit cell consists of 13 transition metal atoms and retains the compact CDW cluster, thereby facilitating the generation of flat bands. However, we find that, distinct from the DS, the ACDS structure is noncentrosymmetric. More specifically, unlike the DS structure [Fig. 1(c)], where the arrangement of chalcogen atoms maintains inversion symmetry, the ACDS exhibits different bonding network patterns in the top and bottom chalcogenide layers [Fig. 1(d)]. This leads to the explicitly broken inversion symmetry. We will show that this broken inversion symmetry, which was unnoticed in our previous work [48], is essential in understanding the electronic states of the ACDS materials.

Notably, our DFT calculations show that the energy difference between DS and ACDS structures is only several meV per atom (see Table S1 [27]). Consequently, it is natural to expect that ACDS is readily synthesized experimentally under appropriate conditions. Indeed, we believe that ACDS is already realized in several monolayer 1T-TMD materials [41–43]. For example, in [41], the STM images exhibit a single bright protrusion surrounded by six smaller protrusions. This feature is inconsistent with the DS structure and better explained by the ACDS. Similarly, the ACDS structure can account for several other STM images [42,43], which we summarize in Fig. S1 [27].

Band structure.—The introduction of the ACDS in 1T-MX_2 leads to an intriguing electronic band structure with several notable features, as depicted in Figs. 2, 3, and S2 [27]. First, one can observe the emergence of flat bands within the CDW gap. The bandwidth of the flat bands is around 80–120 meV, larger than those in the DS cases (around 20 meV). Nonetheless, the flat band states in the ACDS remain well localized in space [see Figs. S2(c) and S2(d) [27]] and are half filled. Furthermore, as apparent from Fig. 2, due to the broken inversion symmetry, the flat bands exhibit Rashba-type spin splitting.

Spin Hall conductivity.—An exceptional interplay of the strong SOC and the large density of states of the flat bands in the ACDS structure can give rise to the giant SHC. Because of the dimensionality of the system and the nature of the Rashba SOC, the sole nontrivial component of the SHC tensor is $\sigma_{xy}^{S_z}$. For example, in TaS_2 (Fig. 2), when the system is gated to tune the Fermi level between the flat bands, the estimated SHC of the monolayer can reach as high as $\sim 0.1(e^2/\hbar)$. When converted to values in 3D bulk [27], it corresponds to $\sim 3 \times 10^4 (\hbar/e)(\Omega m)^{-1}$, surpassing that of the pristine TaS_2, other TMD, and intrinsic spin Hall materials [49–51]. Notably, this giant SHC comes along with the energy splitting between the flat bands, which is larger than the room temperature. The energy splitting reaches as high as 40 meV near the band maximum points and roughly 30 meV around the saddlelike regions (Fig. 2), enabling the effective operation of potential spin devices at room temperature. Other ACDS TMDs exhibit similar strengths of SHC as TaS_2 (see Fig. S4 [27]).

$DFT + U$ calculation.—In the DS, the $5d_{z^2}$ electron in flat bands experiences substantial on-site Coulomb interaction of 1–2 eV, resulting in a Mott insulator [52,53]. Notably, the effective strength of the correlation U and Mott characteristics can vary significantly, depending on stacking [54–56], termination [53,57,58], substrates [19,41], and strain [59]. We expect that the same applies to the ACDS structure, while the effect of the electronic correlation is generally expected to be significant due to the presence of the

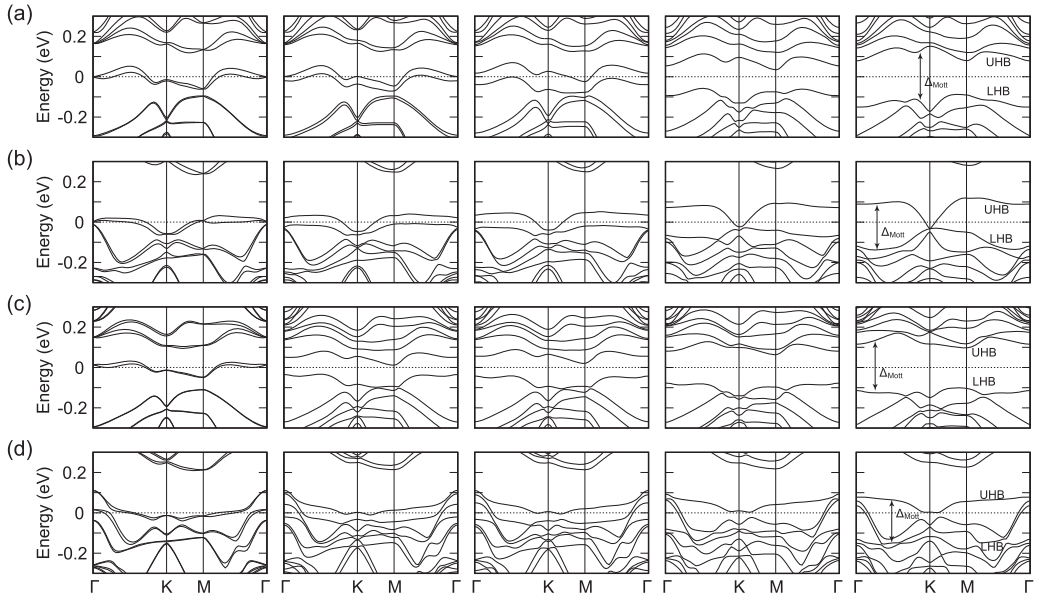

FIG. 3. DFT + U calculation of ACDS 1T-TMD. We depict the band structures for $U = 0$, 0.8, 1, 2, and 3 eV (from left to right) for (a) TaS_2, (b) $TaSe_2$, (c) NbS_2, and (d) $NbSe_2$, respectively.

flat bands. Hence, to comprehensively investigate diverse experimental possibilities, we performed DFT + U calculations for a wide range of U (Fig. 3).

In NbS_2 and TaS_2, where there are no states adjacent to the flat band, we observe that the flat bands gradually split in energy, leading to the formation of the lower and upper Hubbard bands at the moderate strength of the correlation $U \lesssim 1$ eV [Figs. 3(a) and 3(c)]. This clearly manifests the transition from a half-filled metal to a trivial Mott insulator. On the other hand, $TaSe_2$ and $NbSe_2$ present distinct possibilities due to the neighboring bands near the flat bands. In $TaSe_2$ [Fig. 3(b)], the hybridization of the flat bands with neighboring states leads to a topological Mott insulator with the first Chern number of 1 [27]. In $NbSe_2$ [Fig. 3(d)], the flat bands remain relatively buried beneath other bands, which allows the system to maintain its metallic character. However, when U reaches the larger values, $U \gtrsim 2$ eV, the flat bands in both $TaSe_2$ and $NbSe_2$ slowly start to develop a trivial energy gap between them. This energy splitting between the flat bands subsequently leads to the suppression of the density of states near the Fermi level [27].

Remarkably, previous STM experiments [41–43], which reported images consistent with the ACDS, have unveiled the presence of substantial spectral gaps at the Fermi level. While a more systematic investigation is desirable to fully comprehend the nature of the observed gaps, these observations indicate the importance of electronic correlation and possibly the emergence of Mott insulators in these half-filled systems.

Spin model.—Motivated by our DFT + U calculations and spectral gaps observed in experiments [41–43], we derive an effective spin model by expanding around the deep Mott limit $U \gg \max\{t_1, t_2, t_3, \lambda_R\}$ (t_k is the kth neighbor hopping and λ_R is the Rashba SOC) [27]:

$$H = J_1 \sum_{\langle i,j \rangle} \mathbf{S}_i \cdot \mathbf{S}_j + J_2 \sum_{\langle\langle i,j \rangle\rangle} \mathbf{S}_i \cdot \mathbf{S}_j + J_3 \sum_{\langle\langle\langle i,j \rangle\rangle\rangle} \mathbf{S}_i \cdot \mathbf{S}_j + \sum_{\langle i,j \rangle} [J_\parallel (\mathbf{r}_{ij} \cdot \mathbf{S}_i)(\mathbf{r}_{ij} \cdot \mathbf{S}_j) - D \mathbf{r}_{ij} \cdot (\mathbf{S}_i \times \mathbf{S}_j)]. \quad (1)$$

The parameters in Eq. (1) are determined by the hopping and SOC strengths, for example, $J_1 = 4(t_1^2 - \lambda_R^2)/U$. Their explicit values can be found in [27]. The further neighbor terms and higher-order corrections are typically orders of magnitude smaller and, thus, ignored [27]. $\mathbf{S}_i$ is the spin-1/2 moment at site i, and $\langle i, j \rangle$ refers to nearest-neighbor pairs. $\mathbf{r}_{ij}$ is the unit vector directed from the site i to the site j. Similarly, $\langle\langle i, j \rangle\rangle$ and $\langle\langle\langle i, j \rangle\rangle\rangle$ refer to second- and third-neighbor pairs, respectively.

Magnetic phase diagram.—Using variational Monte Carlo (VMC) [60–62] calculations and the Luttinger-Tisza method [63,64], we draw the phase diagram [Fig. 4(a)] of Eq. (1) in terms of $\{J_2/J_1^{(0)}, J_3/J_1^{(0)}, \lambda_R/t_1\}$ with $J_1^{(0)} = 4t_1^2/U$. This is a standard approach in computing phase diagrams in spin Hamiltonians; see, for example, [65]. We append some details on calculation of the phase diagram in [27]. The Rashba SOC λ_R controls the strength of both the $J_\parallel$ and D terms. We normalize the parameters by setting $J_1^{(0)} = t_1 = 1$ from here on.

For sufficiently large values of $\{\lambda_R, J_2, J_3\}$, classical magnetic orders prevail. These orders are denoted as

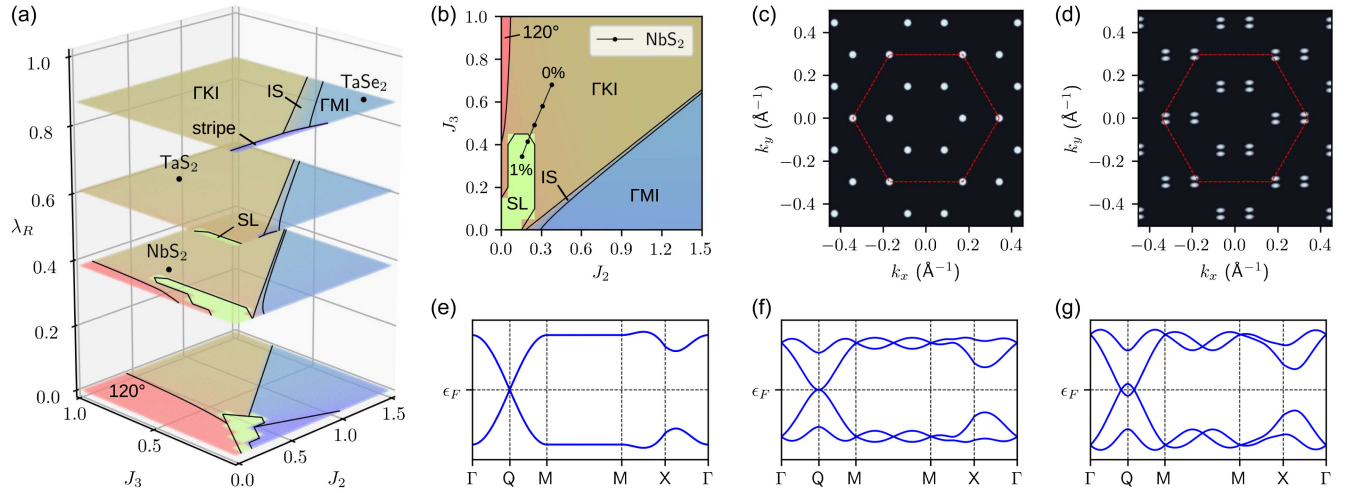

FIG. 4. Magnetic phase diagrams and spin liquids. (a) $\{J_2, J_3, \lambda_R\}$ and (b) $\{J_2, J_3, \lambda_R = 0.45\}$ VMC phase diagrams in units of $J_1^{(0)} = t_1 = 1$. In (a), the locations of TaS_2, $TaSe_2$, and NbS_2 are identified as black circles. In (b), NbS_2 with the strain 0%, 0.25%, 0.5%, 0.75%, and 1% are marked as the black circles. (c) and *(d)* represent the calculated STM signals (in arbitrary units) of the fully symmetric U1B11 state and nematic Dirac spin liquid, respectively. We followed [66] in calculating the STM signals of spin liquids [27]. The STM signal in (d) clearly breaks the crystalline rotational symmetry unlike (c). When calculating (c) and (d), we used the parameters of NbS_2 at 1% strain and tuned the voltage bias of STM to be right above the charge gap. We depict spinon band structures of (e) U1B11 spin liquid without SOC, (f) U1B11 state with SOC Eq. (1), and (g) nematic Dirac spin liquid.

the 120°, stripe, ΓKI, ΓMI, and incommensurate spiral (IS) orders in Fig. 4(a). Their real-space spin configurations can be found in [27]. ΓKI, ΓMI, and IS are stripy, coplanar magnetic orders whose ordering momentum vary continuously with the parameters in Eq. (1). For example, in the ΓKI order, the spins spiral along the momentum, which lies between the Γ and K points in the Brillouin zone. The appearance of these magnetic orders is consistent with prior investigations of the $J_1J_2J_3$ model [65,67–72], which is closely related to Eq. (1).

Remarkably, our VMC simulation has identified the emergence of a spin liquid for lower values of $\{J_2, J_3\}$, labeled as SL in Figs. 4(a) and 4(b). We employed projected fermionic spinon wave functions [73] in the calculation to construct the candidate spin liquid states [27]. Again, our findings regarding the existence and location of the spin liquid phase are in agreement with prior investigations of the $J_1J_2J_3$ model [65,67–72]. Intriguingly, we observed that introducing a small Rashba SOC $\lambda_R/t_1 \lesssim 0.4$ leads to an expansion of the spin liquid region in the phase diagram.

It is noteworthy that NbS_2 resides in close proximity to the spin liquid in the phase diagram [Fig. 4(a)]. The proximity of NbS_2 to the spin liquid phase suggests a tantalizing possibility of engineering a spin liquid state in NbS_2. Remarkably, under the influence of a small, isotropic tensile strain $\lesssim 1\%$, we predict that NbS_2 undergoes a phase transition and become the spin liquid. As the tensile strain increases from 0% to 1%, the second and third neighbor interactions $\{J_2, J_3\}$ decrease and the Rashba SOC increases from $\lambda_R = 0.38$ to $\lambda_R = 0.45$ [27]. While the increment of λ_R does cause a slight suppression of the spin liquid region, the reduction of $\{J_2, J_3\}$ is fast enough that NbS_2 transits to a spin liquid near 0.75% strain. See Fig. 4(b) for the trajectory of $\{J_2, J_3\}$ parameters of NbS_2 under the strain, projected onto the $\lambda_R = 0.45$ plane. We also confirmed that the ACDS structure in NbS_2 is stable against the strain $\lesssim 1\%$ [27]. The other TMD materials are deep inside magnetically ordered phases [Fig. 4(a)].

Nature of spin liquid.—The strong SOC of the ACDS significantly changes the characteristics of the spin liquid state. Specifically, it destabilizes a fully symmetric spin liquid state, leading to an alternative state with the broken crystalline rotational symmetry.

In the absence of SOC, previous studies established the emergence of a symmetric U(1) Dirac spin liquid, which we refer as the U1B11 state [27], in the $J_1J_2J_3$ model [65,68–72,74]. This state is characterized by two Dirac spinons and artificial gauge photons, with each Dirac cone exhibiting double degeneracy due to spin-rotational symmetry [Fig. 4(e)]. We extended this U1B11 state to incorporate SOC and observed that it remains energetically favored over other symmetric U(1) spin liquids. The SOC, however, continuously deforms the spinon band structure from doubly degenerate Dirac cones [Fig. 4(e)] to nondegenerate quadratic band touchings [Fig. 4(f)]. It is well known that quadratic band touching is unstable against repulsive interactions, leading to symmetry-broken states [75]. Guided by previous literature on the instabilities of the quadratic band touching [75–77], we additionally considered five symmetry-broken descendants of the U1B11 state and

compared their energies within the VMC simulation [27]. Among the candidates, the U(1) nematic Dirac spin liquid, a spin liquid with spontaneously broken crystalline rotational symmetry, has the lowest energy than the fully symmetry U1B11 state and other candidates. In particular, strained NbS_2 is in the nematic Dirac spin liquid phase [Fig. 4(b)], whose broken rotational symmetry can be manifested in STM signals [Figs. 4(c) and 4(d)]. The corresponding real-space STM images can be found in [27].

Conclusions.—We have demonstrated that ACDS TMDs showcase a fascinating array of intriguing emergent quantum phenomena, notably including giant spin Hall conductivity, interaction-enabled topological Chern bands, and strain-engineered nematic spin liquids. The pivotal factor in understanding of these phenomena lies in the broken inversion symmetry inherent to the ACDS structure, resulting in flat bands with strong SOC.

Remarkably, these emergent quantum phenomena are anticipated to manifest within the readily accessible ACDS samples [41–43]. By juxtaposing the experimentally probed density of states [41–43] with our DFT + U calculations, we could deduce the appropriate U values for these ACDS samples, thereby unveiling their emergent properties [27]. For instance, our analysis reveals that ACDS TaS_2 exhibits a U value of 2.8 eV, resulting in a trivial Mott insulator characterized by ΓKI magnetic order. Similarly, $TaSe_2$ realizes a topological Mott insulator, while $NbSe_2$ demonstrates the giant SHC, and NbS_2 exhibits a nematic spin liquid [27]. These findings present a compelling opportunity for further experimental exploration to validate our theoretical predictions and shed light on the intriguing physics of ACDS materials.

We are grateful to Hyun-Woo Lee and Young-Woo Son for valuable discussions. C.-E. A. and G. Y. C. are supported by Samsung Science and Technology Foundation under Project No. SSTF-BA2002-05. C.-E. A. and G. Y. C. are supported by the NRF of Korea (Grants No. RS-2023-00208291, No. 2023M3K5A1094810, and No. 2023M3K5A1094813) funded by the Korean Government (MSIT). K.-H. J. acknowledges the support from the Institute for Basic Science (Grant No. IBS-R014-Y1). C.-E. A. and G. Y. C. acknowledge the support by the Air Force Office of Scientific Research under Grant No. FA2386-22-1-4061. A. G. is supported by the NRF of Korea (Grants No. 2021R1C1C1010429 and No. 2023M3K5A1094813). Y. B. K. is supported by the Natural Sciences and Engineering Council of Canada, the Center for Quantum Materials at the University of Toronto, Simons Fellowship, and Guggenheim Fellowship. G. Y. C., J. W. P., and H. W. Y. are supported by Institute of Basic Science under project code IBS-R014-D1.

*These authors contributed equally to this letter.
†arago@jnu.ac.kr
‡yongbaek.kim@utoronto.ca
§gilyoungcho@postech.ac.kr

[1] K. F. Mak, K. He, J. Shan, and T. F. Heinz, Nat. Nanotechnol. **7**, 494 (2012).
[2] X. Xu, W. Yao, D. Xiao, and T. F. Heinz, Nat. Phys. **10**, 343 (2014).
[3] J. M. Lu, O. Zheliuk, I. Leermakers, N. F. Q. Yuan, U. Zeitler, K. T. Law, and J. T. Ye, Science **350**, 1353 (2015).
[4] Y. Yu, F. Yang, X. F. Lu, Y. J. Yan, Y.-H. Cho, L. Ma, X. Niu, S. Kim, Y.-W. Son, D. Feng *et al.*, Nat. Nanotechnol. **10**, 270 (2015).
[5] J. W. Park, G. Y. Cho, J. Lee, and H. W. Yeom, Nat. Commun. **10**, 4038 (2019).
[6] J. M. Lee, C. Geng, J. W. Park, M. Oshikawa, S.-S. Lee, H. W. Yeom, and G. Y. Cho, Phys. Rev. Lett. **124**, 137002 (2020).
[7] Y. Liu, D.-F. Shao, L. J. Li, W. J. Lu, X. D. Zhu, P. Tong, R. C. Xiao, L. S. Ling, C. Y. Xi, L. Pi *et al.*, Phys. Rev. B **94**, 045131 (2016).
[8] B. Sipos, A. F. Kusmartseva, A. Akrap, H. Berger, L. Forro, and E. Tutis, Nat. Mater. **7**, 960 (2008).
[9] K. Rossnagel, J. Phys. Condens. Matter **23**, 213001 (2011).
[10] L. Ma, C. Ye, Y. Yu, X. F. Lu, X. Niu, S. Kim, D. Feng, D. Tomanek, Y.-W. Son, X. H. Chen, and Y. Zhang, Nat. Commun. **7**, 10956 (2016).
[11] Y. Nakata, K. Sugawara, R. Shimizu, Y. Okada, P. Han, T. Hitosugi, K. Ueno, T. Sato, and T. Takahashi, NPG Asia Mater. **8**, e321 (2016).
[12] S. Qiao, X. Li, N. Wang, W. Ruan, C. Ye, P. Cai, Z. Hao, H. Yao, X. Chen, J. Wu, Y. Wang, and Z. Liu, Phys. Rev. X **7**, 041054 (2017).
[13] L. Liu, H. Yang, Y. Huang, X. Song, Q. Zhang, Z. Huang, Y. Hou, Y. Chen, Z. Xu, T. Zhang *et al.*, Nat. Commun. **12**, 1978 (2021).
[14] J. Jung, K.-H. Jin, J. Kim, and H. W. Yeom, Nano Lett. **23**, 8029 (2023).
[15] X. Qian, J. Liu, L. Fu, and J. Li, Science **346**, 1344 (2014).
[16] S. Wu, V. Fatemi, Q. D. Gibson, K. Watanabe, T. Taniguchi, R. J. Cava, and P. Jarillo-Herrero, Science **359**, 76 (2018).
[17] K. T. Law and P. A. Lee, Proc. Natl. Acad. Sci. U.S.A. **114**, 6996 (2017).
[18] W.-Y. He, X. Y. Xu, G. Chen, K. T. Law, and P. A. Lee, Phys. Rev. Lett. **121**, 046401 (2018).
[19] Y. Chen, W. Ruan, M. Wu, S. Tang, H. Ryu, H.-Z. Tsai, R. Lee, S. Kahn, F. Liou, C. Jia, O. R. Albertini, H. Xiong, T. Jia, Z. Liu, J. A. Sobota, A. Y. Liu, J. E. Moore, Z.-X. Shen, S. G. Louie, S.-K. Mo, and M. F. Crommie, Nat. Phys. **16**, 218 (2020).
[20] W. Ruan, Y. Chen, S. Tang, J. Hwang, H.-Z. Tsai, R. L. Lee, M. Wu, H. Ryu, S. Kahn, F. Liou, C. Jia, A. Aikawa, C. Hwang, F. Wang, Y. Choi, S. G. Louie, P. A. Lee, Z.-X. Shen, S.-K. Mo, and M. F. Crommie, Nat. Phys. **17**, 1154 (2021).
[21] Y. Nakata, K. Sugawara, A. Chainani, H. Oka, C. Bao, S. Zhou, P.-Y. Chuang, C.-M. Cheng, T. Kawakami, Y. Saruta, T. Fukumura, S. Zhou, T. Takahashi, and T. Sato, Nat. Commun. **12**, 5873 (2021).

[22] J. Wilson, F. D. Salvo, and S. Mahajan, Adv. Phys. **24**, 117 (1975).
[23] P. Fazekas and E. Tosatti, Physica (Amsterdam) **99B+C**, 183 (1980).
[24] L. Stojchevska, I. Vaskivskyi, T. Mertelj, P. Kusar, D. Svetin, S. Brazovskii, and D. Mihailovic, Science **344**, 177 (2014).
[25] T. Ritschel, J. Trinckauf, K. Koepernik, B. Buechner, M. V. Zimmermann, H. Berger, Y. I. Joe, P. Abbamonte, and J. Geck, Nat. Phys. **11**, 328 (2015).
[26] D. Cho, S. Cheon, K.-S. Kim, S.-H. Lee, Y.-H. Cho, S.-W. Cheong, and H. W. Yeom, Nat. Commun. **7**, 10453 (2016).
[27] See Supplemental Material at http://link.aps.org/supplemental/10.1103/PhysRevLett.132.226401, which includes Refs. [28–40], for detailed discussion of previous experiments, numerical simulation methodology, and our results.
[28] G. Kresse and J. Furthmüller, Phys. Rev. B **54**, 11169 (1996).
[29] J. P. Perdew, K. Burke, and M. Ernzerhof, Phys. Rev. Lett. **77**, 3865 (1996).
[30] S. L. Dudarev, G. A. Botton, S. Y. Savrasov, C. J. Humphreys, and A. P. Sutton, Phys. Rev. B **57**, 1505 (1998).
[31] A. A. Mostofi, J. R. Yates, Y.-S. Lee, I. Souza, D. Vanderbilt, and N. Marzari, Comput. Phys. Commun. **178**, 685 (2008).
[32] M. Gradhand, D. V. Fedorov, F. Pientka, P. Zahn, I. Mertig, and B. L. Gyoerffy, J. Phys. Condens. Mater. **24**, 213202 (2012).
[33] G. Y. Guo, Y. Yao, and Q. Niu, Phys. Rev. Lett. **94**, 226601 (2005).
[34] A. H. MacDonald, S. M. Girvin, and D. Yoshioka, Phys. Rev. B **37**, 9753 (1988).
[35] P. Weinberg and M. Bukov, SciPost Phys. **2**, 003 (2017).
[36] T. Dodds, S. Bhattacharjee, and Y. B. Kim, Phys. Rev. B **88**, 224413 (2013).
[37] S. Bieri, C. Lhuillier, and L. Messio, Phys. Rev. B **93**, 094437 (2016).
[38] T. Fukui, Y. Hatsugai, and H. Suzuki, J. Phys. Soc. Jpn. **74**, 1674 (2005).
[39] M. Liu, J. Leveillee, S. Lu, J. Yu, H. Kim, C. Tian, Y. Shi, K. Lai, C. Zhang, F. Giustino, and C.-K. Shih, Sci. Adv. **7**, eabi6339 (2021).
[40] J. Lee, K.-H. Jin, A. Catuneanu, A. Go, J. Jung, C. Won, S.-W. Cheong, J. Kim, F. Liu, H.-Y. Kee, and H. W. Yeom, Phys. Rev. Lett. **125**, 096403 (2020).
[41] H. Lin, W. Huang, K. Zhao, S. Qiao, Z. Liu, J. Wu, X. Chen, and S.-H. Ji, Nano Res. **13**, 133 (2020).
[42] A. Luican-Mayer, Y. Zhang, A. DiLullo, Y. Li, B. Fisher, S. E. Ulloa, and S.-W. Hla, Nanoscale **11**, 22351 (2019).
[43] Z.-Y. Liu, S. Qiao, B. Huang, Q.-Y. Tang, Z.-H. Ling, W.-H. Zhang, H.-N. Xia, X. Liao, H. Shi, W.-H. Mao, G.-L. Zhu, J.-T. Lu, and Y.-S. Fu, Nano Lett. **21**, 7005 (2021).
[44] G. Gye, E. Oh, and H. W. Yeom, Phys. Rev. Lett. **122**, 016403 (2019).
[45] M. Liu, C. Wu, Z. Liu, Z. Wang, D.-X. Yao, and D. Zhong, Nano Res. **13**, 1733 (2020).
[46] H. Tan, Y. Liu, Z. Wang, and B. Yan, Phys. Rev. Lett. **127**, 046401 (2021).
[47] Y. Bai, T. Jian, Z. Pan, J. Deng, X. Lin, C. Zhu, D. Huo, Z. Cheng, Y. Liu, P. Cui, Z. Zhang, Q. Zou, and C. Zhang, Nano Lett. **23**, 2107 (2023).
[48] J. W. Park and H. W. Yeom, ACS Nano **17**, 17041 (2023).
[49] H. Xu, J. Wei, H. Zhou, J. Feng, T. Xu, H. Du, C. He, Y. Huang, J. Zhang, Y. Liu, H.-C. Wu, C. Guo, X. Wang, Y. Guang, H. Wei, Y. Peng, W. Jiang, G. Yu, and X. Han, Adv. Mater. **32**, 2000513 (2020).
[50] W. Feng, Y. Yao, W. Zhu, J. Zhou, W. Yao, and D. Xiao, Phys. Rev. B **86**, 165108 (2012).
[51] C. K. Safeer, J. Ingla-Aynes, F. Herling, J. H. Garcia, M. Vila, N. Ontoso, M. Reyes Calvo, S. Roche, L. E. Hueso, and F. Casanova, Nano Lett. **19**, 1074 (2019).
[52] P. Darancet, A. J. Millis, and C. A. Marianetti, Phys. Rev. B **90**, 045134 (2014).
[53] J. Lee, K.-H. Jin, and H. W. Yeom, Phys. Rev. Lett. **126**, 196405 (2021).
[54] S.-H. Lee, J. S. Goh, and D. Cho, Phys. Rev. Lett. **122**, 106404 (2019).
[55] Y. D. Wang, W. L. Yao, Z. M. Xin, T. T. Han, Z. G. Wang, L. Chen, C. Cai, Y. Li, and Y. Zhang, Nat. Commun. **11**, 4215 (2020).
[56] Z. Wu, K. Bu, W. Zhang, Y. Fei, Y. Zheng, J. Gao, X. Luo, Z. Liu, Y.-P. Sun, and Y. Yin, Phys. Rev. B **105**, 035109 (2022).
[57] C. J. Butler, M. Yoshida, T. Hanaguri, and Y. Iwasa, Nat. Commun. **11**, 2477 (2020).
[58] F. Petocchi, C. W. Nicholson, B. Salzmann, D. Pasquier, O. V. Yazyev, C. Monney, and P. Werner, Phys. Rev. Lett. **129**, 016402 (2022).
[59] K. Zhang, C. Si, C.-S. Lian, J. Zhou, and Z. Sun, J. Mater. Chem. C **8**, 9742 (2020).
[60] C. Gros, D. Poilblanc, T. Rice, and F. Zhang, Physica (Amsterdam) **153C**, 543 (1988).
[61] C. Gros, Ann. Phys. (Leipzig) **189**, 53 (1989).
[62] B. Edegger, V. N. Muthukumar, and C. Gros, Adv. Phys. **56**, 927 (2007).
[63] J. Luttinger and L. Tisza, Phys. Rev. **70**, 954 (1946).
[64] D. B. Litvin, Physica (Amsterdam) **77**, 205 (1974).
[65] J. Iaconis, C.-X. Liu, G. Halász, and L. Balents, SciPost Phys. **4**, 003 (2018).
[66] E. Tang, M. P. A. Fisher, and P. A. Lee, Phys. Rev. B **87**, 045119 (2013).
[67] S.-S. Gong, W. Zheng, M. Lee, Y.-M. Lu, and D. N. Sheng, Phys. Rev. B **100**, 241111(R) (2019).
[68] Y. Iqbal, W.-J. Hu, R. Thomale, D. Poilblanc, and F. Becca, Phys. Rev. B **93**, 144411 (2016).
[69] F. Ferrari and F. Becca, Phys. Rev. X **9**, 031026 (2019).
[70] Z. Zhu, P. A. Maksimov, S. R. White, and A. L. Chernyshev, Phys. Rev. Lett. **120**, 207203 (2018).
[71] N. E. Sherman, M. Dupont, and J. E. Moore, Phys. Rev. B **107**, 165146 (2023).
[72] M. Drescher, L. Vanderstraeten, R. Moessner, and F. Pollmann, Phys. Rev. B **108**, L220401 (2023).
[73] X.-G. Wen, Phys. Rev. B **65**, 165113 (2002).
[74] S. Hu, W. Zhu, S. Eggert, and Y.-C. He, Phys. Rev. Lett. **123**, 207203 (2019).
[75] K. Sun, H. Yao, E. Fradkin, and S. A. Kivelson, Phys. Rev. Lett. **103**, 046811 (2009).
[76] S. Uebelacker and C. Honerkamp, Phys. Rev. B **84**, 205122 (2011).
[77] W. Zhu, S.-S. Gong, T.-S. Zeng, L. Fu, and D. N. Sheng, Phys. Rev. Lett. **117**, 096402 (2016).